Proceedings of ASME 2016 International Design Engineering Technical Conferences and Computers and Information in Engineering Conference
IDETC/CIE 2016
August 21-24, 2016, Charlotte, North Carolina

IDETC2016-60477

DESIGN, FABRICATION, EXPERIMENTAL ANALYSIS, AND TEST FLIGHT OF AN ORIGAMI-BASED FIXED-WING AERIAL VEHICLE: μPLANE

Siamak G. Faal
Fuchen Chen
Weijia Tao
Shadi T. Kalat
Soft Robotics Laboratory
Worcester Polytechnic Institute
Worcester, Massachusetts 01609
Email: {sghorbanifaal, fchen, wtao, stasdighikalat}@wpi.edu

Payam Razavi
Center for Holographic Studies and Laser micro-mechaTronics
Department of Mechanical Engineering
Worcester Polytechnic Institute
Worcester, Massachusetts 01609
Email: prazavi@wpi.edu

Vahideh Eshaghian *
Aerospace Engineering Department
Amirkabir University of Technology
Tehran, Iran
Email: v.eshaghian@campus.tu-berlin.de

Cagdas D. Onal†
Soft Robotics Laboratory
Worcester Polytechnic Institute
Worcester, Massachusetts 01609
Email: cdonal@wpi.edu

ABSTRACT

This article covers details the design, fabrication, experimental analysis, and first flight tests of μPlane, an origami-inspired aerial vehicle. μPlane is a monoplane with a straight wing planform that has a wingspan of 580 millimeters and can reach a maximum linear velocity of 6.12 meters-per-second. The body of the μPlane is fabricated by folding a single, unified crease pattern which includes all the sections required to construct the wing, tail, fuselage, and connection ports for external components, such as actuators and batteries. The wing of the plane utilizes a cambered profile to generate the required lift force. An optimization problem is formulated to find a solution to the set of constraints that provides the desired camber form. To validate the proposed design, a 3D scan of the top surface of the wing is accrued using a high-resolution fringe projection system. Finally, the flight performance and stability of μPlane are tested in both indoor and outdoor environments.

1 Introduction

Small-scale and micro aerial vehicles (MAV) are getting more attention from researchers due to their usability in highly cluttered environments [1, 2]. Their small dimensions allow utilization of small-scale aerial vehicles in tasks which require dexterity. Examples include, but are not limited to: situational awareness [3], search and rescue [4], and object manipulation [5]. The limited payload capacity of MAVs, which is a consequence of their small size [6], can be compensated by utilizing them in multi-agent or swarm configurations.

This article introduces design steps and fabrication of a fully functional small-scale origami fixed-wing aerial vehicle, μPlane (see Fig. 1). Inspired by origami techniques and the art of making paper airplanes, μPlane is designed to be fabricated very easily and yet provide the required shape for aerodynamic performance

*Vahideh Eshaghian is currently with the Space Engineering Program at the Technical University of Berlin

†Address all correspondence to this author.

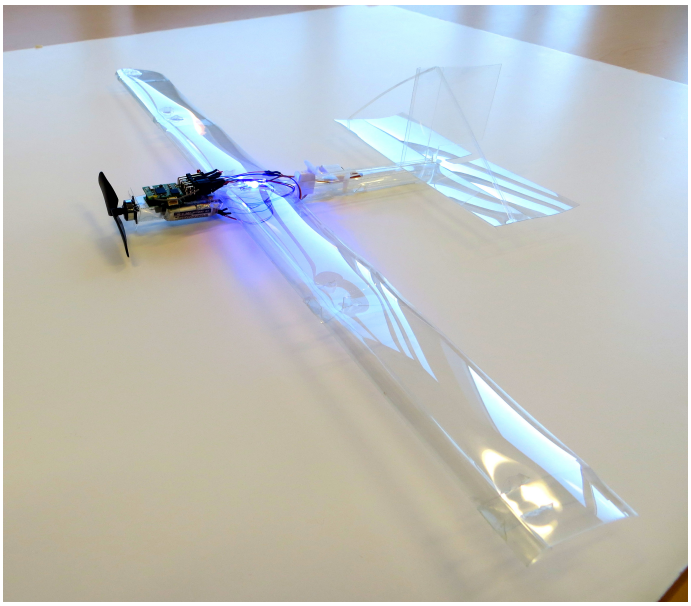

FIGURE 1. The fully assembled prototype of μPlane.

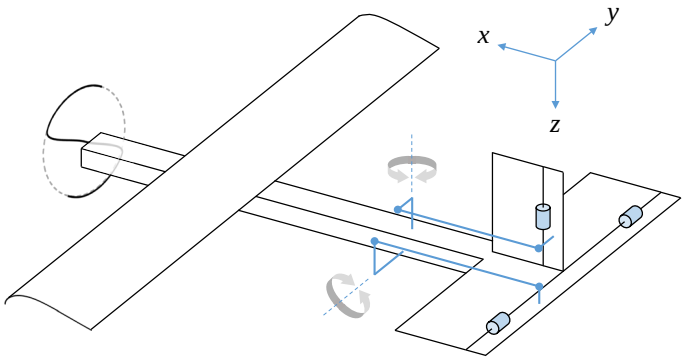

FIGURE 2. Conceptual design of μPlane. The blue lines represent the parallel mechanisms used to control the rotations of rudder and elevator. The corresponding revolute joints that connect the control surfaces to the tail and fin are depicted with blue cylinders. Note that this figure is not drawn to scale.

as explained in [7]. Moreover, due to the nature of materials used to fabricate origami-based objects, the structure provides necessary compliance to tolerate impacts and collisions [8]. The inherent mechanical compliance of the structure also significantly helps with isolating the on-board sensory infrastructure (e.g. inertial measurement units) from mechanical vibrations that are introduced by the electric motors and propellers. Since the union of the crease patterns for different parts of μPlane form a simple closed curve, The crease pattern for each μPlane can be fabricated on a single sheet, stacked in layers and manufactured on site to reduce storage requirements and transportation costs.

TABLE 1. Flight conditions, wing, tail and airfoil parameters

Description	Parameter	Value
Total Mass (including payload)	M	60 g
Nominal velocity	v_n	10 m/s
Air density	ρ_{air}	1.1839 kg/m^3
Chord	c	50 mm
Wing span	b	580 mm
Airfoil thickness*	t/c	0.5 %
Maximum camber*	f/c	15 %
location of maximum camber*†	x_f/c	26 %

* The values are presented in percentage of the chord length
† The location of maximum camber is measured from the leading edge of the airfoil.

To validate the method used in design of the curved plate, a 3D scan of the fabricated wing is acquired using a fringe projection system. The wing and the fuselage are tested under realistic loading conditions to ensure their structural rigidity. Test flights of the platform are performed to ensure its functionality. To our knowledge, μPlane is the first fully origami-based controllable small-scaled fixed-wing aircraft that can fly both in indoor and outdoor environments. The main contributions of this article are: design of a crease pattern for a fixed wing aircraft with a cambered wing airfoil; design process used to generate a curved segment with a desired profile; embedding all the fasteners required for the external components in the crease pattern to eliminate the need for any external fasteners.

The rest of the article is organized as follows. Section 2 discusses the general structure of the μPlane, the conceptual design, and the airfoil shape. The crease pattern design and the optimization problem to find a set of constraining connections that ensures the desired cambered profile are discussed in Section 3. The fabrication process, external components, and final physical dimensions of the fabricated prototype are covered in Section 4. Section 5 describes the procedure and results of 3D scanning the fabricated airfoil, test flights and experiments to find the maximum linear velocity of μPlane. The article is concluded with discussions and future work in Section 6.

2 Conceptual design

μPlane is a monoplane with straight wing planform which utilizes a rudder and an elevator to control the yaw and pitch motions, respectively. To reduce the complexity of the crease pattern and focus on the design process, μPlane concept does not use control surfaces on the wing (e.g. ailerons, flaps or spoilers).

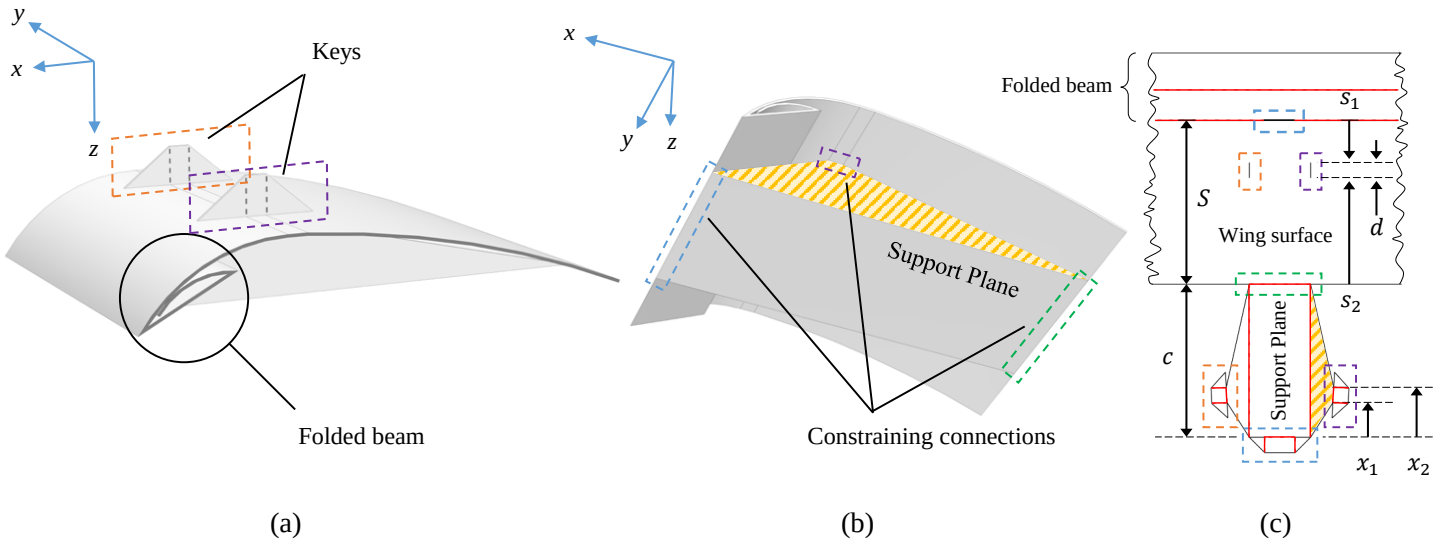

FIGURE 3. Two different views of the same section of the origami wing and the corresponding crease pattern. (a) x-z view. (b) x-y view of the same segment (c) The corresponding crease pattern. Black and red colors illustrate cut and fold lines respectively. The regions that are indicated by dashed rectangles construct the constraining connections which form the camber. The color coding is used to indicate the same regions in all three views.

If required, these control surfaces can be included by following the same design criteria explained in Section 3 which is an extension to the origami-based design process we previously presented in [8]. A conceptual overview of the μPlane structure and its control surfaces are illustrated in Fig. 2. As depicted in this figure, the fuselage of μPlane is a straight beam that supports the actuators, propeller, wing and tail. The control electronics and batteries are also carried by the fuselage. Two parallelogram mechanisms [9] are used to translate the motion of two servo motors, located on the fuselage, to the rudder and elevator plates. These mechanisms allow further control on the position of the center of mass (CoM) of μPlane by adjusting the distance between the servos and the tail.

By searching through the available airfoils based on shape and thickness requirements that are convenient for an origami-based design, GOE462 airfoil (maximum thickness = 11% at 9.9% chord; maximum camber = 13.4% at 29.9% chord) is chosen as the base airfoil of the wing. The airfoil parameters are further trimmed to simplify the crease pattern design and reduce total weight of the platform. The tail of μplane utilizes flat plates as airfoils. Table 1 presents all the associated parameters of the wing, tail and considered flight conditions.

3 Crease pattern design

The crease pattern design of μPlane follows the procedures we introduced in [8]. As discussed in [8], an origami based structure can be designed by unifying the crease patterns of basic structures, which form the links and joints of a kinematic system. These basic structures include triangular hollow beams, flexural revolute joints, key-and-slot fasteners, and insertion locks. While triangular beams are used to support loads, flexures provide functionality of revolute joints. To maintain physical integrity of the folds, key-slot fasteners and insertion locks can then be added to the crease patterns. The complete crease pattern of μPlane is illustrated in Fig. 7. The design details for each section of the structure are discussed in the following subsections.

3.1 Wing design

Instead of folding flat surfaces into polygonal forms, μPlane wing is shaped by curving a surface in the desired camber form. This design method is in contrast to most origami-based designs introduced so far [10–13]. Curving a surface to shape the wing guarantees smoothness of the airfoil and eliminates the formation of sharp edges as a result of discrete fold lines. The curved surface of the wing is designed by constraining a thin segment of a flexible material between two (flexural) pin joints that are closer to each other than the length of the segment. Thus, forcing the segment to form an arc with a constant radius. This property of the thin plates is used in an optimization problem to determine a set of locations to constrain the cambered segment of the wing.

Figure 3 illustrates two views of a wing section with the corresponding crease pattern. In this figure the constraining connections are depicted in dashed regions. The constraining connection sets, each composed of two key-slot connections and a fold, constrain the wing surface from 4 different points and push it to form the desired camber profile. These points are p_0 = origin, p_1, p_2 and $p_3 = (c, 0)$ as depicted in Fig. 4. The distance and

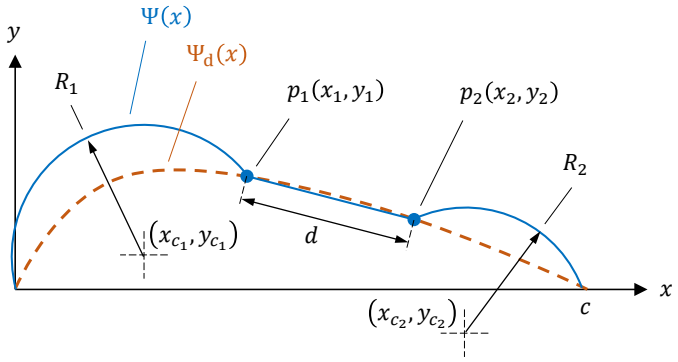

FIGURE 4. Parameters and variables used in the formulation of the optimization problem (1). The dashed orange line shows the desired curve, Ψ_d, and blue solid curve illustrate Ψ curve as described in section 3.1.

the form of the camber between p_1, p_2 is directly controlled by key-slot connections (illustrated with dashed orange and purple regions in Figure 3(c)). The points p_0 and p_3 are constrained by a key-slot connection (dashed blue region in Figure 3(c)) and a fold (dashed green region in Figure 3(c)), respectively. The locations of these four points are determined by solving the optimization problem discussed in this section. Each two sets of constraining connections are supported by a support plane, which determines the distance between p_0 and p_3. μPlane utilizes five discrete support planes to maintain the desired wing profile over the span as depicted in Fig. 7. To increase the rigidity of the wing across its span and constructing the lower surface of the airfoil, a semi-elliptical beam that is formed by two consequent folds is introduced to the crease pattern.

The details of formulating the optimization problem is presented in what follows. The design and dependent variables used in this formulation are depicted in Fig. 4. The goal is to minimize the root mean square (rms) between the desired camber profile, $\Psi_d(x)$, and a curve that is constructed by joining two arcs with a straight line, $\Psi(x)$. The set of design variables v is defined as: $v = \{x_1, x_2, R_1, R_2\}$. Thus, the problem can be formulated as:

$$\underset{v\in U,\ x\in X}{\text{minimize}}\ \ \text{rms}(\Psi_d(x) - \Psi(x)), \tag{1}$$

where $U = \{v \in \mathbb{R}^4 \ : \ v \geq 0,\ v_2 > v_1\}$ and $X = \{x \in \mathbb{R} \ : \ 0 \leq x \leq c\}$. The curve $\Psi_d(x)$ is defined as a polynomial that represents the desired camber of the airfoil; $\Psi(x)$ is the curve obtained by joining two arcs to the line segment between points p_1 and p_2. Variables R_1 and R_2 represent the radii of the two arcs. The piecewise function that defines $\Psi(x)$ is defined as:

$$\Psi(x) = \begin{cases} \sqrt{{R_1}^2 - (x - x_{c_1})^2} + y_{c_1} & 0 \leq x < x_1 \\ (x - x_1)(y_2 - y_1)/(x_2 - x_1) + y_1 & x_1 \leq x \leq x_2 \\ \sqrt{{R_2}^2 - (x - x_{c_2})^2} + y_{c_2} & x_2 < x \leq x_3 \end{cases} \tag{2}$$

where $y_i = \Psi_d(x_i)$ for $i \in \{1,2\}$. The center points $c_i = (x_{ci}, y_{ci})$ are defined as:

$$\begin{bmatrix} x_{c_i} \\ y_{c_i} \end{bmatrix} = \left[\frac{D_i}{2}\ R_i \cos(\sin^{-1}(\frac{D_i}{2R_i}))\right] \begin{bmatrix} \cos(\phi_i) & \sin(\phi_i) \\ \sin(\phi_i) & -\cos(\phi_i) \end{bmatrix}, \tag{3}$$

where $D_1 = \|p_1\|$, $D_2 = \|p_3 - p_2\|$, $\phi_1 = \text{atan2}(y_1, x_1)$ and $\phi_2 = \text{atan2}(-y_2, x_3 - x_2)$. The genetic algorithm optimization toolbox of MATLAB software is used to find a solution for the formulated optimization problem with the maximum $\max(\text{rms}(\Psi_d(x) - \Psi(x))) = -0.271\%$ (located at $x = 2\%$ of the chord length from the leading edge). After obtaining the values for the design variables, they can be mapped to the parameters used in the crease pattern design (as depicted in Fig. 3(c)) by the following mappings:

$$s_i = 2R_i \sin^{-1}(\frac{D_i}{2R_i}). \tag{4}$$

Thus, the arc length that is needed for the wing surface is $S = s_1 + s_2 + \| p_1 - p_2 \|$.

3.2 Fuselage and tail design

The fuselage of μPlane is a triangular beam that carries all the sections and components of the platform. The crease pattern of the fuselage includes all the necessary connection ports for the external components; thus, the final assembly of the system does not require any external fasteners (e.g. screws, nuts, tape, or glue). The connection port that connects the propeller motor (an outrunner brushless DC (BLDC)) to the fuselage is illustrated in Fig. 5. The highlighted regions in this figure show the embedded triangular hooks which lock the motor to the fuselage [8] by pressing the motor against them (insertion locks). The control electronics are simply inserted inside the beam. The batteries are connected to the fuselage by using the four ribbons located behind the BLDC motor as depicted in Fig. 7.

The tail of μPlane, illustrated in Fig. 6, is composed of: horizontal and vertical stabilizers; rudder and elevator and the corresponding parallelogram mechanisms used for their actuation. The two servo motors that actuate the rudder and elevator are directly mounted on the fuselage with the same technique that is used for the propeller motor (illustrated in Fig. 5). Two small

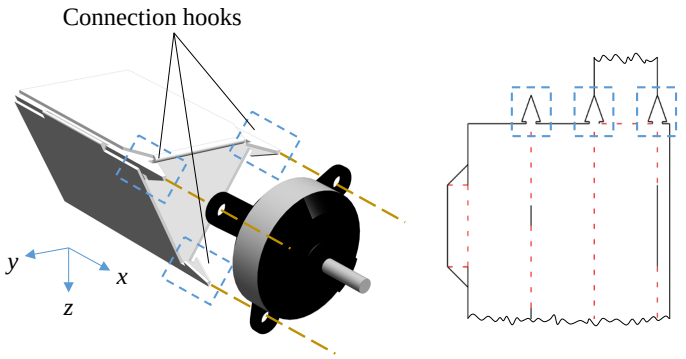

FIGURE 5. Connection port of the BLDC motor to the fuselage and the corresponding crease pattern. The hooks that are used to lock the motor to the fuselage are indicated with blue dashed regions.

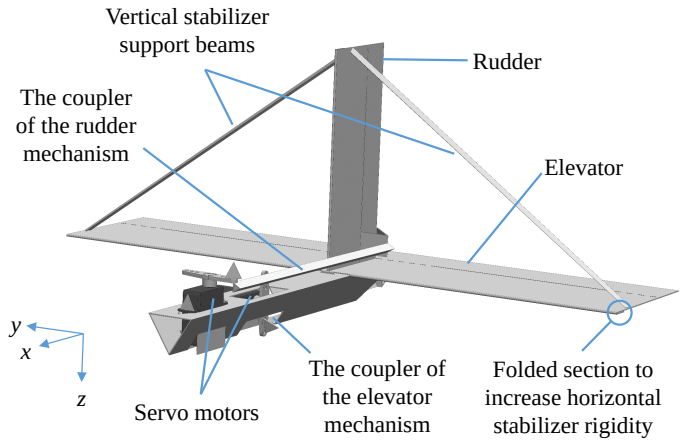

FIGURE 6. The tail design of the μPlane. Two triangular beams are added to the stabilizers to increase their rigidity and reduce the induced vibrations during flight. Two servo motors that actuate the rudder and elevator are connected to the fuselage using folded hooks that are inserted into screw holes of the motors. Two triangular beams are used as the coupler links of the rudder and elevator mechanisms.

triangular beams connect the top of the vertical stabilizer to the tips of the horizontal stabilizer. These beams are used to increase the rigidity of the tail and reduce the induced vibrations during flight. The coupler links of the rudder and elevator mechanism are also two triangular beams that are extended from the control surfaces to the corresponding servo motor arms. Similar to the wing design, the leading edges of the stabilizers are folded back to increase their stiffness.

4 Fabrication

The fabrication process starts with laser cutting the crease pattern on a sheet of PET with 0.1778 mm (0.007 in) thickness.

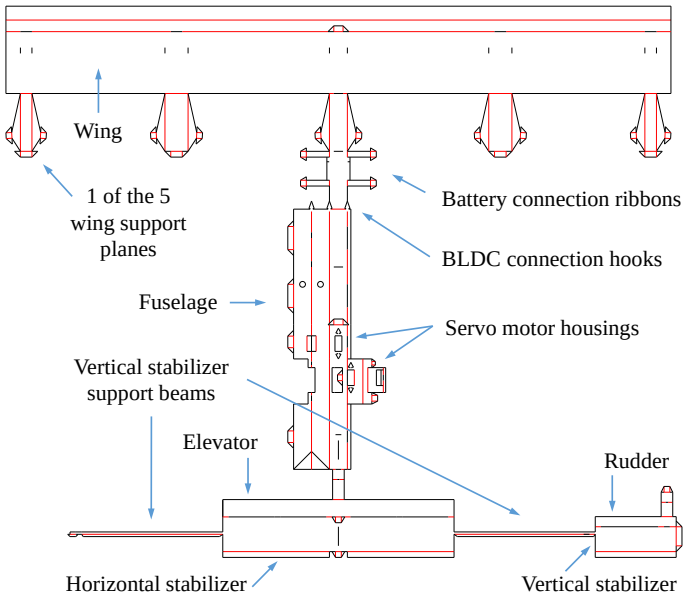

FIGURE 7. The complete crease pattern of μPlane. Red and black colors are used to indicate fold and cut lines, receptively.

Laser cutting the full pattern takes approximately 30 minutes. The crease pattern is then manually folded to form the final shape of the platform. While the servo motors used for the rudder and elevator mechanism need to be assembled inside the fuselage during the folding phase, the rest of the external components can be added to the platform after folding is completed. The complete fabrication of the platform takes less than 1 hour. μPlane uses a 3-inch diameter propeller with a 2-inch pitch that is connected to a 7000-rpm/V BLDC motor to generate the required thrust. The BLDC motor weighs 3.1 grams and it can fit in a $13 \times 13 \times 16$ mm^3 box. The rudder and elevator mechanism are driven by two miniature servo motors that each weigh less than 2 grams and provide an output torque of 0.17 kg·cm. A use controls the plane via a DX6i 6-channel transmitter that is paired to an on-board AR6210 6-channel receiver. While the servo motors are directly connected to the receiver, the BLDC motor uses a 0.7-gram, 3-amperes BLDC driver to convert the received servo pulse commands into motor drive voltages. The complete system is powered by two 200 mAh, 1-cell lithium polymer batteries that each weigh 5.2 grams. The fully assembled platform weighs 46 grams and can fit into a $58 \times 33 \times 9$ cm^3 box.

5 Experimental analysis

In order to validate the design, the performance of the fabricated platform is tested under a range of scenarios. The initial test is conducted on the form of the wing airfoil. The 3D shape of the airfoil was acquired using a high-resolution fringe projection system (100 μm resolution). The scanning method

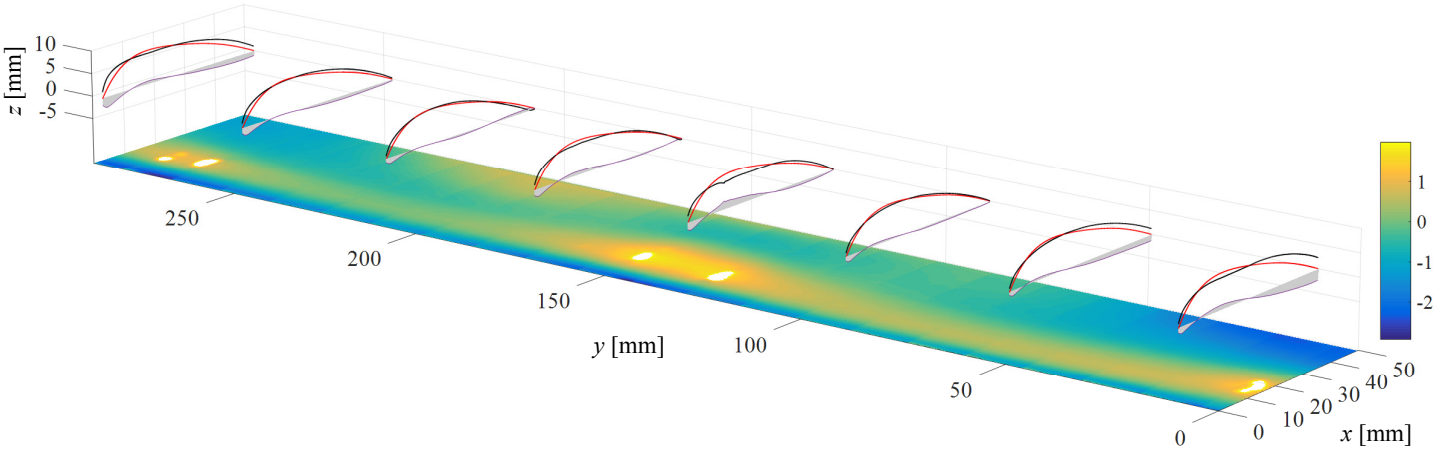

FIGURE 8. The result of the 3D scanning the top surface of half of the wing. Black and red lines illustrate the accrued wing profiles and the desired cambers at 8 different sections, respectively. The gray area under each sample shows the error between the two profiles. The colormap on the x-y plane illustrates the error between the desired and fabricated wing profile for the entire half wing. The white regions in the colormap are due to faulty readings that are caused by the keys.

is based on projecting known sinusoidal phase-shifted patterns on the surface of the object and acquiring the corresponding images. Then, by analyzing multiple known phase-shifted images (in this case four $\pi/2$ phase shifts), the 3D shape of the object is reconstructed. The resolution of the system can vary by the resolution of the fringes on the object surface. In the experiment, eight fringes-per-square-inch are projected to the wing.

Figure 8 summarizes the results of this experiment. The desired and fabricated profiles at 8 different locations on one half of the wing are presented as samples. The black lines illustrate the curve of the fabricated wing and are compared with the desired cambers depicted in red. For each sample, the gray area under the curves illustrates the error between the desired and acquired cambers. The colormap on the x-y plane depicts the error for the entire half of the wing. The white areas in the colormap represent faulty readings that are caused by the keys.

To validate the rigidity of the origami-based wing for withstanding lift forces during flight, the wing structure was supported at both ends and a point force was applied to the middle of the wing. The wing structure could tolerate forces up to 0.981 N (100 grams), which is more than twice the weight of the platform. Although this experiment does not directly represent the aerodynamic forces applied to the wing, it provides a good estimate on the rigidity of the wing structure.

To measure the maximum velocity and battery lifetime of the system, μPlane is tied to a string from its center of mass and attached to a pole sufficiently above the ground. Then, the angular velocity of the propeller is gradually increased to its maximum value. As a result, the plane went through a circular motion around the pole. This condition is kept for about 2 minutes at which the batteries run out of charge. The maximum angular velocity of the vehicle (measured as π rad/s) and the radius of its circular motion are then used to calculate the maximum linear velocity of the plane to be 6.12 m/s (22.03 km/h). Finally, test flights are performed in indoor and outdoor environments. These tests are meant to measure the overall stability and control of the system. Snapshots of the μPlane during an indoor flight are shown in Fig. 9. Since the body of the platform is transparent (due to the transparency of the PET sheets used for fabrication), dashed blue circles are added to highlight the location of the aircraft at each snapshot.

6 Conclusions

This work focuses on the design process, fabrication, and experimental analysis of an origami-inspired fixed-wing aerial vehicle, μPlane. Since the wings of the plane needs to have smooth surfaces, to construct the defined airfoil shape, an optimization problem is formulated. The results of optimization are used to design and fabricate the crease pattern for the wing to realize a smooth cambered profile when folded. The final shape of the airfoil is then verified by 3D scanning the top surface of the wing using a high resolution fringe projection system. The scanning results prove that the origami wing forms the desired cambered shape with good accuracy. The platform is then tested both in indoor and outdoor environments to validate the performance of the system. To reduce the complexity of the design, μPlane does not have any control surfaces on the wing to actively control the roll angle. This causes the plane to lose stability when it is subjected to a relatively strong cross wind. Incorporating corresponding control surfaces to increase the controllability and stability of the platform and further reducing its size and weight

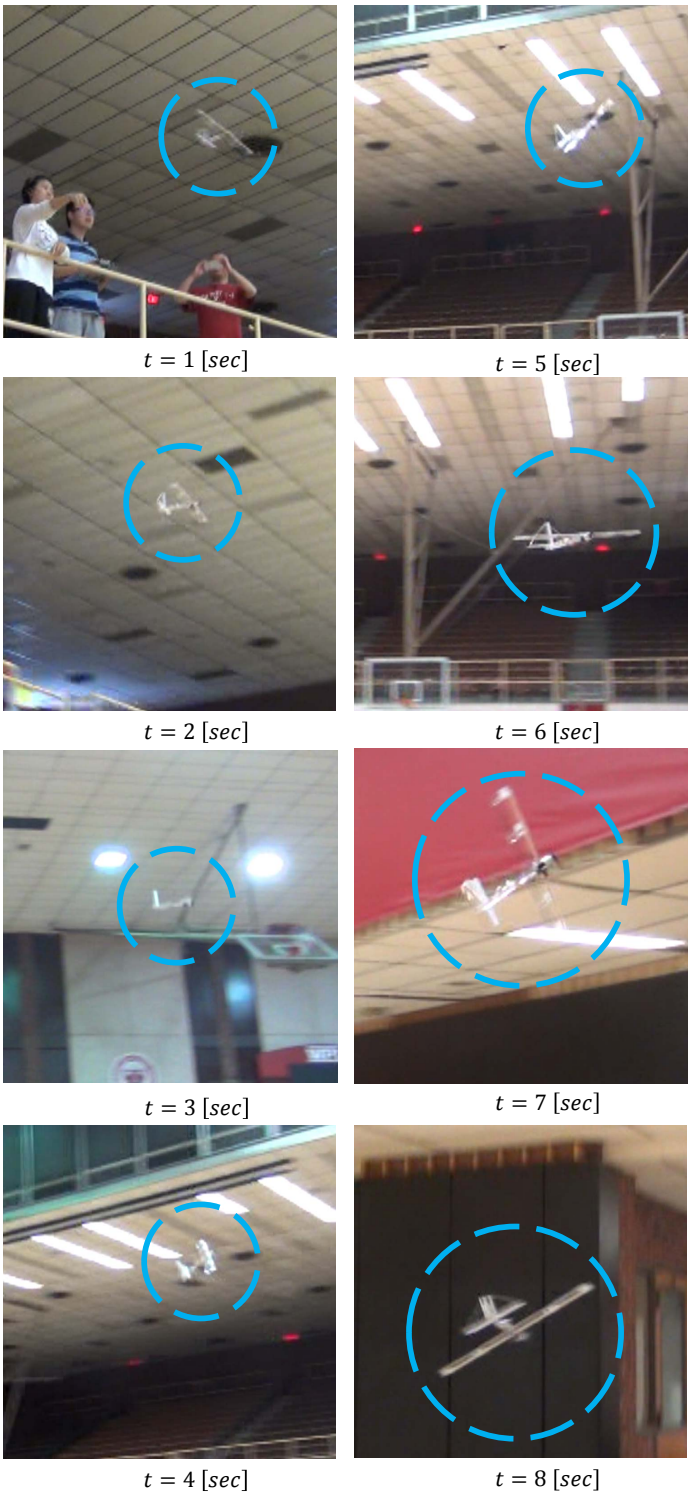

FIGURE 9. Indoor test flight of the μPlane. Snapshots show the platform as it maneuvers around the camera. The blue dashed circles are used to show the location of the platform on each image. The time values are measured in seconds.

are some of the future work of this research.

ACKNOWLEDGMENTS

The authors would like to thank Cosme Furlong, a research faculty at the Center of Holographic Studies and Laser micro-mechaTronics (CHSLT/NEST) laboratories at Worcester Polytechnic Institute, for providing the facilities required for 3D scanning of the wing. Authors also would like to acknowledge Saber Jahanpour for his generous help and thoughtful comments on this manuscript.

REFERENCES

[1] V. Kumar and N. Michael, "Opportunities and challenges with autonomous micro aerial vehicles," *The International Journal of Robotics Research*, vol. 31, no. 11, pp. 1279–1291, 2012.

[2] K. Nonami, F. Kendoul, S. Suzuki, W. Wang, and D. Nakazawa, *Autonomous Flying Robots: Unmanned Aerial Vehicles and Micro Aerial Vehicles*. Springer Science & Business Media, 2010.

[3] J. M. Grasmeyer, M. T. Keennon, *et al.*, "Development of the black widow micro air vehicle.," *Progress in Astronautics and aeronautics*, vol. 195, pp. 519–535, 2001.

[4] R. R. Murphy, E. Steimle, C. Griffin, C. Cullins, M. Hall, and K. Pratt, "Cooperative use of unmanned sea surface and micro aerial vehicles at hurricane wilma," *Journal of Field Robotics*, vol. 25, no. 3, pp. 164–180, 2008.

[5] J. Thomas, G. Loianno, J. Polin, K. Sreenath, and V. Kumar, "Toward autonomous avian-inspired grasping for micro aerial vehicles," *Bioinspiration & biomimetics*, vol. 9, no. 2, p. 025010, 2014.

[6] D. J. Pines and F. Bohorquez, "Challenges facing future micro-air-vehicle development," *Journal of aircraft*, vol. 43, no. 2, pp. 290–305, 2006.

[7] W. Shyy and R. Smith, "A study of flexible airfoil aerodynamics with application to micro aerial vehicles," *AIAA Paper*, vol. 1933, 1997.

[8] S. G. Faal, F. Chen, W. Tao, M. Agheli, S. Tasdighikalat, and C. D. Onal, "Hierarchical kinematic design of foldable hexapedal locomotion platforms," *JMR*, vol. 3, no. 4L3, p. 1, 2015.

[9] P. W. Jensen, *Classical and modern mechanisms for engineers and inventors*. Dekker, 1991.

[10] D. E. Soltero, B. J. Julian, C. D. Onal, and D. Rus, "A lightweight modular 12-dof print-and-fold hexapod," in *Intelligent Robots and Systems (IROS), 2013 IEEE/RSJ International Conference on*, pp. 1465–1471, IEEE, 2013.

[11] M. Agheli, S. G. Faal, F. Chen, H. Gong, and C. D. Onal, "Design and fabrication of a foldable hexapod robot towards experimental swarm applications," in *Robotics and*

Automation (ICRA), 2014 IEEE International Conference on, pp. 2971–2976, IEEE, 2014.

[12] S. M. Felton, M. T. Tolley, C. D. Onal, D. Rus, and R. J. Wood, "Robot self-assembly by folding: A printed inchworm robot," in *Robotics and Automation (ICRA), 2013 IEEE International Conference on*, pp. 277–282, IEEE, 2013.

[13] S. T. Kalat, S. G. Faal, U. Celik, and C. D. Onal, "Tribot: A minimally-actuated accessible holonomic hexapedal locomotion platform," in *Intelligent Robots and Systems (IROS), 2015 IEEE/RSJ International Conference on*, pp. 6292–6297, IEEE, 2015.